Published in final edited form as:
J Bone Miner Res. 2014 January ; 29(1): . doi:10.1002/jbmr.2012.

3D Assessment of Cortical Bone Porosity and Tissue Mineral Density Using High-Resolution Micro-CT: Effects of Resolution and Threshold Method

Paolo E. Palacio-Mancheno, M.S.[1,*], **Adriana I. Larriera, M.S.**[1,*], **Stephen B. Doty, Ph.D.**[2], **Luis Cardoso, Ph.D.**[1], and **Susannah P. Fritton, Ph.D.**[1,+]

[1]Department of Biomedical Engineering, City College of New York, New York, NY, USA

[2]Research Division, Hospital for Special Surgery, New York, NY USA

Abstract

Current micro-CT systems allow scanning bone at resolutions capable of three-dimensional characterization of intracortical vascular porosity and osteocyte lacunae. However, the scanning and reconstruction parameters along with the image segmentation method affect the accuracy of the measurements. In this study, the effects of scanning resolution and image threshold method in quantifying small features of cortical bone (vascular porosity, vascular canal diameter and separation, lacunar porosity and density, and tissue mineral density) were analyzed. Cortical bone from the tibia of Sprague-Dawley rats was scanned at 1-μm and 4-μm resolutions, reconstructions were density-calibrated, and volumes of interest were segmented using approaches based on edge-detection or histogram analysis. With 1-μm resolution scans, the osteocyte lacunar spaces could be visualized, and it was possible to separate the lacunar porosity from the vascular porosity. At 4-μm resolution, the vascular porosity and vascular canal diameter were underestimated, and osteocyte lacunae were not effectively detected, whereas the vascular canal separation and tissue mineral density were overestimated compared to 1-μm resolution. Resolution had a much greater effect on the measurements than did threshold method, with partial volume effects at resolutions coarser than 2 μm demonstrated in two separate analyses, one of which assessed the effect of resolution on an object of known size with similar architecture to a vascular pore. Although there was little difference when using the edge-detection versus histogram-based threshold approaches, edge-detection was somewhat more effective in delineating canal architecture at finer resolutions (1 – 2 μm). In addition, use of a high-resolution (1-μm) density-based threshold on lower resolution (4-μm) density-calibrated images was not effective in improving the lower-resolution measurements. In conclusion, if measuring cortical vascular microarchitecture, especially in small animals, a micro-CT resolution of 1 – 2 μm is appropriate, while a resolution of at least 1 μm is necessary when assessing osteocyte lacunar porosity.

Keywords

intracortical porosity; vascular porosity; micro-CT; resolution; partial volume effect

[+]**Corresponding author:** Susannah P. Fritton, Ph.D., Department of Biomedical Engineering, City College of New York, 160 Convent Ave., New York, NY 10031, Phone: 212-650-5213, Fax: 212-650-6727, fritton@ccny.cuny.edu.
[*]These authors contributed equally to the study

Disclosures
All authors state that they have no conflicts of interest.

Introduction

Cortical porosity and tissue mineral density contribute to the overall mechanical properties of bone, particularly to bone stiffness and strength[1–5]. The intracortical vascular porosity associated with the bone blood vessels and the lacunar-canalicular porosity that surrounds osteocytes also contribute to bone's transport phenomena[6]. The relaxation of fluid pressure surrounding osteocytes is dependent on the vascular canals, which act as a low pressure reservoir[7,8]. Bone interstitial fluid flow is also dependent on the mechanical strains of the solid phase during loading, with deformations related to the cortical and trabecular bone compressibility[9]. Because mechanically induced solute transport ensures the metabolic function of osteocytes[10,11], it is important to accurately quantify cortical bone porosities and tissue mineral density, particularly during disease states that may alter bone microstructure.

Current methods to analyze bone microarchitecture in general, and cortical porosity in particular, utilize light and confocal microscopy as well as micro-computed tomography (μCT)[12,13]. Histomorphometric approaches are widely used, but they involve the destruction of the sample and may create artifacts during the processing and sectioning of calcified tissue[14]. μCT is a non-destructive, 3D imaging technique in which several of the standard histomorphometry methods used to measure both trabecular and cortical bone microarchitecture have been automated, allowing analysis of relatively large bone volume samples with high correlation between histology and μCT-imaged morphology[15,16]. Tissue mineral density (TMD) can also be obtained from μCT once images are calibrated to density using known standards[16]. Synchrotron radiation-based μCT yields high-resolution 3D images[5,17], but the field of view is limited and the devices are not widely available. While commercial μCT scanners are widely used research tools, until recently the limited spatial resolution of these scanners has been a barrier to the accurate measurement of cortical bone microarchitecture, particularly when studying small animal models. The last few years have seen an improvement of the resolution of commercial μCT systems, and now experiments can be performed reaching nominal resolutions as high as 1 μm. Image processing and histomorphometric analysis at this level of resolution are, however, time and computer intensive tasks. Therefore, it is important to determine which resolution is adequate for accurate and effective quantification of cortical bone porosity and TMD.

The accuracy of μCT measurements associated with small microarchitectural features increases as the scanning voxel size decreases; however, at high resolutions, the field of view becomes extremely small, limiting the possibility of scanning volumes of interest on the order of several mm^3. Furthermore, segmentation of bone and porosities is still user dependent; thresholds are obtained by means of local or global inspection of the object structure and the grayscale histogram, or by using a semi-automated intensity detection algorithm to generate boundaries between interfaces[18, 19]. The most commonly used segmentation method is to apply a global threshold; however, unless global thresholding is used after beam hardening effects have been corrected, local segmentation is recommended[18]. It is possible that segmentation limitations could be mitigated by high-resolution scanning, corrections for beam hardening, and the implementation of a density-based thresholding method.

The goal of this study was to provide guidance for the appropriate nominal scanning resolution and threshold approach to use for quantification of cortical bone porosity using high-resolution μCT. The specific aims were (1) to investigate the effects of resolution and image thresholding method on three-dimensional measurements of intracortical bone properties, including vascular canal porosity, vascular canal diameter and separation, osteocyte lacunar porosity and density, and TMD; (2) to investigate whether a density-based

threshold value obtained at high resolution can be used as an appropriate threshold value on density-calibrated images at lower resolution; and (3) to investigate the role of partial volume effects on μCT measurements of small architectural features.

Materials and Methods

Sample preparation

Cortical bone from the tibia of skeletally mature Sprague Dawley rats was analyzed, and permission for the study was granted by the Institutional Animal Care and Use Committee at the Hospital for Special Surgery. As part of a larger study to evaluate bone changes due to estrogen deficiency, rats were subjected to sham ovariectomy surgery at twenty weeks of age, where the ovaries were surgically exposed without being removed (n=6, Harlan Laboratories). At twenty-six weeks of age, the animals were euthanized and the right tibiae were harvested and placed in 10% neutral buffered formalin for 48 hours. After fixation, the tibiae were placed in 70% ethanol and stored at 4° C until imaging. Before scanning, bone samples were brought to room temperature while immersed in phosphate buffered saline within a custom low X-ray attenuation plastic holder that held each bone in place for scanning.

Micro-computed tomography imaging

To assess the effect of resolution, tibiae were scanned using a μCT system (SkyScan 1172, Bruker microCT, Belgium) where projections (4000 × 4000 pixels) of the anterior proximal tibia were acquired with nominal isotropic resolutions of 1 μm and 4 μm. The 1-μm nominal resolution was the highest resolution possible by the μCT system, but the field of view (FOV) was limited to 4 mm × 4 mm, thus requiring scanning of a selected region of the proximal tibia. The 4-μm nominal resolution (16 mm × 16 mm FOV) was chosen because it allowed scanning of the entire tibia and it is in the mid-range of μCT resolutions recently used in the literature[5,17,20,21]. To reduce the spatial variability in the X-ray intensity profiles from the center to the edges of the images, the proximal anterior region of each tibia was aligned to match the axis of rotation of the scanner, thus placing the anterior region of the bone in the center of the FOV for each scanning resolution. Images were acquired using a 10 MP digital detector of 11 μm physical pixel size. A 10 W power energy setting (100 kV and 100 μA) and a 0.5 mm aluminum filter were used to minimize beam hardening effects by utilizing mostly high energy photons and filtering low energy photons. An alignment procedure and flat-field detector calibration were performed prior to scanning to minimize ring artifacts and increase signal-to-noise ratio. 180° scans were performed with five X-ray projections acquired every 0.3 degrees, each with an exposure time of 5301 ms (1 μm) or 1767 ms (4 μm). For the Skyscan system, these scanning parameters, at each respective resolution, were chosen to optimize the signal-to-noise ratio and contrast of the images. The total scan time was approximately 5 h at 1-μm resolution and 2 h at 4-μm resolution, although the 1-μm scans imaged only 1/64th of the volume of the 4-μm scans. To calibrate for TMD, hydroxyapatite rods (2 mm radius, densities of 0.25 and 0.75 gHA/cm^3) and volumes of saline and air were also scanned at 1-μm and 4-μm resolutions with the same parameters described above.

Image reconstruction and density calibration

A modified back-projection reconstruction algorithm (v.1.6.5, NRecon, SkyScan, Bruker microCT, Belgium)[22] was used to generate cross-sectional images from the X-ray projections. Images were optimized using a standard post-alignment compensation algorithm, treated using a smoothing filter with a Gaussian window kernel (four pixels for 1-μm resolution and one pixel for 4-μm resolution, to maintain the grayscale histogram range equivalent between resolutions), and corrected for ring artifacts. Further beam hardening

correction was achieved using the NRecon software to check that the X-ray intensity profiles across the bone cross-section remained linear. A programmed compensation for baseline intensity available in the NRecon software was employed in the reconstruction of the 1-μm images (both samples and calibration phantoms) because the FOV for the 1-μm scans was smaller than the proximal tibial diameter and thus there was tissue outside the FOV as well as a lack of air and saline at some scanning angles.

Using the hydroxyapatite calibration scans, the grayscale dataset was transformed into Hounsfield units (HU) by assigning an HU value of 0 to the average grayscale index of saline, and an HU value of −1000 to black pixels (air). Next, average HU values for the two mineralized phantoms (0.25 and 0.75 gHA/cm^3) were used to create a linear relationship between HU and mineral density. This was performed separately for the 1-μm and 4-μm datasets using the calibration scan at each corresponding resolution.

Image thresholding

To assess the effect of threshold on cortical porosity and TMD measurements, threshold values were determined using two common approaches: an edge-detection and a histogram-based method. The edge-detection (Edge_Det) algorithm (Canny-Deriche filtering, ImageJ v1.37, National Institutes of Health) discriminates bone from pore by delineating boundaries based on the spatial density gradients. For each bone image dataset and at each resolution, the grayscale images were processed using the edge-detection algorithm, and a threshold was chosen that produced binarized images that best matched the detected pore edges. The histogram-based threshold (Hist) was determined using the histograms of the grayscale image datasets. The two highest peaks from the histogram of each bone's image dataset were identified and a grayscale level corresponding to the lowest point between the peaks, which represents the transition between bone and pore, was selected. The threshold selection using the histogram process was also verified by local inspection of the bone architecture after thresholding. For the six bones analyzed, the coefficient of variation of the threshold was low; hence, for both the Edge_Det and Hist approaches, a single threshold was determined for each tibia and then the average global threshold was used for the group.

In addition to the Edge_Det and Hist threshold methods, an additional analysis was performed to determine whether a density-based threshold value obtained at high resolution (1 μm) could be used to segment bone and canal space in density-calibrated images of lower resolution (4 μm), thus producing an observer-independent threshold in gHA/cm^3. This analysis was completed using both Edge_Det and Hist thresholds obtained from the 1-μm resolution images applied to the 4-μm resolution images.

Quantification of cortical bone microarchitecture and TMD

For each animal, two cylindrical intracortical volumes of interest (VOIs) of 250 μm diameter and 2 mm height were chosen from the anterior proximal tibia starting 1 mm distal to the growth plate. Care was taken to avoid any portion of the medullary cavity space. To quantify cortical bone porosities, vascular canals and osteocyte lacunae were extracted from the VOIs using Mimics software (v14.1.1.1, Materialise, Leuven, Belgium). Compartments representing porosities were created by selecting all voxels with a density value lower (inverse segmentation) than the threshold values previously determined using the Edge_Det or Hist threshold methods, producing large objects (canals), small objects (lacunae), and noise. Using a 3D region-growing operation, the vascular canals were isolated, and 1-voxel sized noise objects were removed using erosion-dilation procedures. Using the CTAn software (v.1.11.0, SkyScan, Bruker microCT, Belgium), osteocyte lacunae were isolated using a 3D despeckled filter that removed objects outside the range of 100 μm^3 to 600 μm^3 in volume[23]. To prevent the addition or removal of voxels on edges and boundaries of all

segmentations, voxel-based operations were limited to the surfaces of the original thresholded images. Also, to prevent edge effects, the first and last images of the VOI stack were discarded from the 3D analysis.

The average vascular canal porosity (Ca.V/TV, %), canal diameter (Ca.Dm, μm), canal separation (Ca.Sp, μm), lacunar porosity (Lc.V/TV, %), and lacunar density (N.Lc/TV, # of lacunae per mm^3) were measured using CTAn. The canal diameter and separation were computed using the "sphere fitting" method developed by Hildebrand and Ruegsegger[24], and lacunar density was quantified as the number of 3D objects per unit volume. In addition to the cortical porosity measurements, the average TMD (gHA/cm^3) was also calculated for each VOI (measured in thresholded images, excluding pores). All parameters were assessed for the two VOIs at each image resolution (1 μm and 4 μm) and threshold method (Edge_Det and Hist). Cortical porosity parameters were also calculated for two subsets of the 250-μm diameter VOIs: the more proximal half (1 mm in height), and the more distal half (1 mm in height) to assess spatial differences within the VOIs.

Assessment of resolution-related partial volume effects

To assess partial volume effects due to decreasing resolution, the diameter of low X-ray attenuation nylon fibers was evaluated at different scanning resolutions. The diameter of the nylon fibers (n=7) was first quantified using high-resolution calipers (Absolute, model 547-520, Mitutoyo Corp, IL, USA). Then the fibers were embedded in a lead-chromate contrast agent (Microfil, Flow Tech, Carver, MA) to produce a structure with an X-ray attenuation similar to that of bone[25] and containing cylinders similar in size to the bone vascular canals. The embedded nylon fibers were scanned at 1-μm, 2-μm, 3-μm, 4-μm, and 8-μm resolutions and reconstructed using the same methodology described above. Exposure times were 5301 ms (1 μm and 8 μm), 1767 ms (3 μm and 4 μm), or 3534 ms (2 μm). Images were optimized using individual standard post-alignment compensation, treated using a smoothing filter with a Gaussian window kernel (four pixels for 1-μm resolution, two pixels for 2-μm resolution, and one pixel for 3-μm and 4-μm resolutions, to maintain the grayscale histogram range equivalent between resolutions). For each of the five resolutions, images were segmented using the Edge_Det and Hist methods as previously described, and the diameter of the nylon fibers was quantified with CTAn using the previously described methods to measure vascular canal diameter.

To further assess the effects of decreasing resolution on the delineation of cortical bone vascular and lacunar pores, the right tibia of an additional female Sprague Dawley rat (twenty-four weeks old; underwent sham ovariectomy at twelve weeks of age) was scanned at 1-μm, 2-μm, 3-μm, 4-μm, and 8-μm resolutions using the same methodology previously described. Baseline intensity compensation in the NRecon software was employed for the 1-μm and 2-μm resolution scans because there was bone tissue outside the FOV and a lack of air and saline at some scanning angles. One cylindrical intracortical VOI of 250 μm diameter and 1 mm height was chosen from the anterior proximal tibia starting 2 mm distal to the growth plate. For each resolution, images were segmented using the Edge_Det and Hist methods, and morphological parameters were quantified using the previously described methods.

Statistical analysis

Differences in cortical microarchitecture and TMD due to resolution (1 μm vs. 4 μm) and thresholding method (Edge_Det vs. Hist) were assessed using a repeated-measures two-way ANOVA followed by Bonferroni's multiple comparison tests with a significance level of $p < 0.05$. Differences in cortical bone microarchitecture and TMD in the 4-μm resolution images thresholded using the density-based threshold obtained at 1-μm resolution were analyzed

using two-tailed paired t-tests (significance level of $p < 0.05$). Comparisons of measurements from the proximal and distal VOIs was also assessed using a two-tailed paired t-test. Changes in measured diameter of the nylon fibers due to changes in resolution were assessed using a repeated-measures one-way ANOVA followed by Bonferroni's multiple comparison tests with a significance level of $p < 0.05$. The normality of the data sets was confirmed before using parametric tests, and Prism software (v.5, GraphPad, CA, USA) was used for all statistical analyses.

Results

A μCT resolution of 1 μm better delineated the microarchitecture of cortical bone compared to 4-μm resolution (Figs. 1 & 2). The 1-μm resolution images produced a more continuous representation of the vascular canal porosity compared to the 4-μm resolution images (Fig. 2a–e). With the 1-μm resolution scans, the osteocyte lacunar spaces could be visualized, and it was possible to separate the lacunar porosity from the vascular porosity during quantification (Fig. 2f).

There were significant differences in the cortical porosity and TMD measurements for the 1-μm and 4-μm resolution images. For both the Edge_Det and Hist thresholds, the 4-μm images had a significantly lower cortical vascular canal porosity (−51 to −73%), a smaller canal diameter (−34 to −39%), a larger canal separation (+23 to +53%), and a slightly higher TMD (+5.3 to +5.8%) compared to the 1-μm images (Fig. 3). In addition, the 4-μm resolution images were too coarse to delineate the osteocyte lacunar porosity and density, which were essentially zero for the 4-μm images (Fig. 3). Comparing the effect of threshold, at 1-μm resolution, there were no differences when applying the two threshold methods because both the Edge_Det and Hist methods resulted in an equivalent threshold of 0.45 gHA/cm^3. At 4-μm resolution, using the Hist threshold (0.81 gHA/cm^3) compared to the Edge_Det threshold (0.63 gHA/cm^3) produced no significant differences in vascular canal porosity, canal diameter, or TMD; however, the Hist threshold resulted in a vascular canal separation somewhat closer to that measured with the 1-μm resolution images (Fig. 3). Applying the high-resolution (1-μm), density-based thresholding value to the lower resolution (4-μm) scans resulted in similar results as the Edge_Det and Hist thresholds: an underestimation of vascular canal porosity (−85%) and canal diameter (−36%) and an overestimation of canal separation (+71%) and TMD (+5%) compared to the 1-μm scans, and lacunar porosity and density were close to zero (Fig. 4).

The values of cortical vascular pore architecture varied spatially within the VOIs, independent of the resolution and threshold method used. For the 1-μm scans, the cortical vascular canal porosity measured for the entire VOI was 4.8 ± 1.1%, with an average of 6.5 ± 1.8% for the proximal half of the VOI significantly higher than the average of 2.7 ± 0.44% for the distal half ($p < 0.05$). The canal diameter measured for the entire VOI was 14.7 ± 1.9 μm, with an average of 18.7 ± 6.1 μm for the proximal half not significantly different from the average of 13.1 ± 1.3 μm for the distal half ($p > 0.05$). The canal separation for the entire VOI was 92.8 ± 10.6 μm, with an average of 78.5 ± 14.9 μm for the proximal half significantly lower than the average of 104 ± 11.2 μm for the distal half ($p < 0.05$).

Independent of anatomical variation within the VOIs, the analysis of variance indicated that of the two imaging factors analyzed (resolution and threshold), resolution was the main source of variation affecting all the studied parameters. For vascular canal porosity, resolution accounted for 75% of the variance, while threshold accounted for only 2%. For canal diameter, 81% of the variance was due to resolution and only 0.4% due to the threshold method. For canal separation, 57% of the variance was due to resolution and 10% due to the threshold method. Analysis of TMD among groups indicated that 48% of the

TMD variance was due to the resolution and only 0.1% due to the threshold method. Finally, resolution accounted for almost 94% of the variance of the lacunar porosity and density, and threshold had no effect on the variance. The only parameter that had a significant interaction between resolution and threshold was canal separation, which also demonstrated a small but significant difference in the 4-μm resolution images thresholded with Edge_Det and Hist (Fig. 3c).

In the analyses of partial volume effects, the nylon fiber diameter measured using μCT decreased with coarser resolution (Fig. 5). Only the fiber diameters measured using 1-μm and 2-μm resolutions and analyzed with the Edge_Det threshold method (24.5 ± 1.2 μm and 24.2 ± 1.3 μm, respectively) were not statistically different from the actual diameter measured using high-resolution calipers (25.3 ± 0.15 μm) (Fig. 5a). The diameter measured using 3-μm (14.2 ± 0.92 μm), 4-μm (13.1 ± 0.89 μm) and 8-μm (non-detectable) resolutions were 44%, 48% and 100% smaller than the actual fiber diameter, respectively. A similar trend was seen with the images analyzed using the Hist threshold method, although the fiber diameters measured using all the scanning resolutions were statistically different from the caliper measurements, including the 1-μm and 2-μm scans (Fig. 5b), indicating that the edge-detection threshold method is more appropriate than the histogram method for vascular canal quantification.

The assessment of partial volume effects using a single tibia scanned at resolutions from 1 – 8 μm also demonstrated that vascular canal diameter, lacunar porosity, and lacunar density decrease with coarser resolution (Fig. 6). The lacunar density and porosity dropped sharply at 3-μm resolution, and were close to zero at 4-μm and 8-μm resolutions. The vascular canal diameter also dropped substantially at 4-μm resolution and was not effectively delineated at 8-μm resolution. This multiple-resolution analysis of a single tibial region highlights that increasing voxel size diminishes the delineation of edges/boundaries of small bone features such as vascular pores and osteocyte lacunae, which leads to a misrepresentation of these architectural parameters.

Discussion

This study was undertaken to provide guidance in choosing an optimal resolution and threshold method capable of accurately characterizing cortical bone microarchitecture and TMD using three-dimensional μCT assessments. Rat bone was scanned at resolutions that included the highest resolution available on a desktop μCT scanner (1 μm), and segmented with two commonly used thresholding methods. Because of the better delineation of small pores, the intracortical bone porosity was significantly greater for 1-μm scans compared to 4-μm scans. The measured values for both the vascular canal porosity and canal diameter were higher in 1-μm scans, and the osteocyte lacunar porosity was measureable, whereas the resolution in 4-μm scans was too coarse to adequately detect the lacunar pores (Figs. 3 & 4).

When comparing resolution and threshold method, resolution was found to be the main source of variation in the measured parameters. The choice of resolution clearly affected the quantification of microarchitectural parameters, with cortical vascular porosity ~100% greater and vascular canal diameter ~50% greater at 1-μm resolution compared to 4-μm resolution. Duvall et al.[26] previously investigated the ability of contrast-enhanced μCT to resolve collateral vessel development after ischemia in a mouse model, and demonstrated that a lower resolution diminished the vessel volume, vessel connectivity and vessel number, indicating the importance of a small voxel size to resolve small caliber vessels. In the present study the nylon fiber analysis demonstrated the reliability of 1-μm and 2-μm resolution μCT images thresholded with an edge-detection method to quantify objects of similar size to bone vascular pores. Caliper measurements of the nylon fiber diameter

demonstrated no statistically significant differences with the fiber diameter measured from 1-μm and 2-μm resolution edge-detected μCT images, whereas the percent difference found by comparing the caliper measurements to μCT measurements at the other image resolutions analyzed (3 to 8 μm) ranged from 44% to 100% (Fig. 5a). The nylon fiber diameter measured using histogram-thresholded μCT images also showed a decrease in diameter as the voxel size increased, but the 1-μm and 2-μm resolution scans did not depict the nylon fiber diameter as effectively as the edge-detected images (Fig. 5b). In addition, the bone analysis at multiple resolutions (1 – 8 μm) demonstrated diminished effectiveness in delineating vascular and lacunar pores with increasing voxel size, with only the 1-μm resolution able to quantify both vascular and lacunar pores (Fig. 6). Overall, these results demonstrate that a low-resolution partial volume effect is the major contributor to μCT quantification errors of small architectural features.

In addition to analyzing two commonly used threshold techniques (a histogram-based approach and an edge-detection approach), the μCT images were also analyzed using a density-based threshold obtained at high resolution to see if this threshold could be used effectively with lower resolution scans. The rationale behind this approach comes from the fact that at high resolution, structural aspects are optimally delineated, so it seems feasible that bone/pore segmentation using a density-based threshold should make the image segmentation independent of the scanning resolution. However, when a single threshold value of 0.45 gHA/cm^3 was applied to the 1-μm and 4-μm resolution scans, significant differences were found in the microarchitecture and TMD measurements (Fig. 4). These differences were largely due to the small features analyzed in this study, and because of the strong influence of partial volume effects at 4-μm resolution, as described above. Thus, using a high-resolution density-based threshold approach to characterize small features was not possible across the studied resolutions.

The values of cortical microarchitectural parameters reported in this study lie within the ranges of values found in the literature, although it should be noted that reported values vary according to species, anatomical location, size of the VOI analyzed, as well as the resolution and threshold used. The average cortical bone vascular porosity of 4.8% found using 1-μm resolution and 1.3% – 2.3% using 4-μm resolution in this study fell within the range of values reported in the literature for rodents (0.5 – 7%) using histomorphometry as well as μCT and synchrotron based X-ray at resolutions ranging from 0.7 to 7 μm[5,17,21,23,27–29]. Also, the 14.7 μm average canal diameter measured using 1-μm resolution and the 9.0 – 9.7 μm canal diameter assessed at 4-μm resolution are similar to the 17.2 μm diameter values found by Britz et al.[21] using 3-μm resolution in the tibial mid-diaphysis of Sprague Dawley rats as well as the 10.3 μm average canal diameter measured in mice by Schneider et al. using 3.7-μm resolution[28]. The 1.5 ± 0.44% lacunar porosity values reported in this study using 1-μm resolution are in close agreement with the 1.3% from Schneider et al. using 0.7-μm resolution in mice[5] and 1.5% from Tommasini et al. using 0.75-μm resolution in rats[23]. Also, the osteocyte lacunar density reported here (68.8 ± 13.2 ×10^3 lacunae per mm^3) is similar to recent μCT volumetric measurements in mice and rats (49.0 ×10^3 to 66.0 ×10^3 lacunae per mm^3)[5,23]. The cortical TMD values found at 1-μm resolution (1.26 gHA/cm^3) and at 4-μm resolution (1.33 –1.34 gHA/cm^3) in the present study are also very similar to the 1.13 – 1.36 g/cm^3 values reported in rodents[17,29,30]. Overall, the range of reported values for cortical microarchitecture demonstrates that there are biological (species, location) and technical (scanning resolution) factors that increase the variability of measurements.

In conclusion, this study demonstrates that a μCT nominal resolution of 1 μm allows quantification of osteocyte lacunar pores (density and porosity) as well as intracortical vascular pores. A scanning resolution of 2 μm may also be effective when assessing vascular

microarchitecture, especially when using an edge-detection thresholding method. Resolutions coarser than 2 μm are not adequate to detect changes in small architectural features of cortical bone, especially when changes (e.g., to a pore surface) may be on the order of a few microns. A disadvantage of using a 1-μm resolution is the increased scanning time, along with the smaller volume of bone that can be imaged in a single scan; in contrast, a resolution of 2 μm (8 mm × 8 mm FOV) could be used to scan a whole bone cross-section, but lacunar quantification would be diminished. While the 4-μm scans did not accurately represent the intracortical porosity because the resolution was too coarse, there are advantages to using a resolution coarser than 1 – 2 μm. Resolutions of 3 – 8 μm (or coarser) could be used to scan an entire rat tibia, which is convenient for 3D modeling of whole bone structure as well as assessing architectural features larger than those studied here (e.g., cortical thickness or trabecular separation). The resolution of the scan should always be chosen based on the size of the structure being analyzed as well as on the size of the expected microarchitecture changes that the experimenter wants to quantify. If measuring cortical vascular porosity, especially in small animals, a μCT resolution of 1 – 2 μm is appropriate, while a resolution of at least 1 μm is necessary when assessing osteocyte lacunar porosity.

Acknowledgments

We would like to thank Yury Borisov, B.E. for his technical assistance. This work was financially supported by NIH/NIAMS (AR052866), NIH/NIA (AG034198), and the NSF/MRI (CBET-0723027). Authors' roles: Study design: LC and SPF. Data collection and analysis: PEPM and AIL. Data interpretation: PEPM, AIL, SBD, LC, and SPF. Drafting manuscript: PEPM, AIL, LC and SPF. Revising manuscript content and approving final version of manuscript: PEPM, AIL, SBD, LC, and SPF. SPF takes responsibility for the integrity of the data analysis. PEPM and AIL contributed equally to this work.

References

1. Schaffler MB, Burr DB. Stiffness of compact bone: effects of porosity and density. J Biomech. 1988; 21:13–16. [PubMed: 3339022]
2. Martin RB. Determinants of the mechanical properties of bones. J Biomech. 1991; 24:79–88. [PubMed: 1842337]
3. McCalden RW, McGeough JA, Barker MB, Court-Brown CM. Age-related changes in the tensile properties of cortical bone. The relative importance of changes in porosity, mineralization, and microstructure. J Bone Joint Surg Am. 1993; 75:1193–1205. [PubMed: 8354678]
4. Wachter NJ, Augat P, Krischak GD, Sarkar MR, Mentzel M, Kinzl L, Claes L. Prediction of strength of cortical bone in vitro by microcomputed tomography. Clin Biomech. 2001; 16:252–256.
5. Schneider P, Stauber M, Voide R, Stampanoni M, Donahue LR, Müller R. Ultrastructural properties in cortical bone vary greatly in two inbred strains of mice as assessed by synchrotron light based micro- and nano-CT. J Bone Miner Res. 2007; 22:1557–1570. [PubMed: 17605631]
6. Piekarski K, Munro M. Transport mechanism operating between blood supply and osteocytes in long bones. Nature. 1977; 269:80–82. [PubMed: 895891]
7. Wang L, Fritton SP, Cowin SC, Weinbaum S. Fluid pressure relaxation depends upon osteonal microstructure: modeling an oscillatory bending experiment. J Biomech. 1999; 32:663–672. [PubMed: 10400353]
8. Goulet GC, Hamilton N, Cooper D, Coombe D, Tran D, Martinuzzi R, Zernicke RF. Influence of vascular porosity on fluid flow and nutrient transport in loaded cortical bone. J Biomech. 2008; 41:2169–2175. [PubMed: 18533159]
9. Cowin SC. Bone poroelasticity. J Biomech. 1999; 32:217–238. [PubMed: 10093022]
10. Knothe Tate ML, Steck R, Forwood MR, Niederer P. In vivo demonstration of load-induced fluid flow in the rat tibia and its potential implications for processes associated with functional adaptation. J Exp Biol. 2000; 203:2737–2745. [PubMed: 10952874]

11. Wang L, Cowin SC, Weinbaum S, Fritton SP. Modeling tracer transport in an osteon under cyclic loading. Ann Biomed Eng. 2000; 28:1200–1209. [PubMed: 11144981]
12. Müller R. Hierarchical microimaging of bone structure and function. Nat Rev Rheumatol. 2009; 5:373–381. [PubMed: 19568252]
13. Cardoso L, Fritton SP, Gailani G, Benalla M, Cowin SC. Advances in assessment of bone porosity, permeability and interstitial fluid flow. J Biomech. 2013; 46:253–265. [PubMed: 23174418]
14. Basillais A, Bensamoun S, Chappard C, Brunet-Imbault B, Lemineur G, Ilharreborde B, Ho Ba Tho MC, Benhamou CL. Three-dimensional characterization of cortical bone microstructure by microcomputed tomography: validation with ultrasonic and microscopic measurements. J Orthop Sci. 2007; 12:141–148. [PubMed: 17393269]
15. Cooper DM, Matyas JR, Katzenberg MA, Hallgrimsson B. Comparison of microcomputed tomographic and microradiographic measurements of cortical bone porosity. Calcif Tissue Int. 2004; 74:437–447. [PubMed: 14961208]
16. Bouxsein ML, Boyd SK, Christiansen BA, Guldberg RE, Jepsen KJ, Müller R. Guidelines for assessment of bone microstructure in rodents using micro-computed tomography. J Bone Miner Res. 2010; 25:1468–1486. [PubMed: 20533309]
17. Matsumoto T, Yoshino M, Asano T, Uesugi K, Todoh M, Tanaka M. Monochromatic synchrotron radiation muCT reveals disuse-mediated canal network rarefaction in cortical bone of growing rat tibiae. J Appl Physiol. 2006; 100:274–280. [PubMed: 16141381]
18. Waarsing JH, Day JS, Weinans H. An improved segmentation method for in-vivo μCT imaging. J Bone Miner Res. 2004; 10:1640–1650. [PubMed: 15355559]
19. Rathnayaka K, Sahama T, Michael MA, Schmutz B. Effects of image segmentation methods on the accuracy of long bone reconstructions. Med Eng Phys. 2011; 33:226–233. [PubMed: 21030288]
20. Cooper D, Turinsky A, Sensen C, Hallgrimsson B. Effect of voxel size on 3D micro-CT analysis of cortical bone porosity. Calcif Tissue Int. 2007; 80:211–219. [PubMed: 17340226]
21. Britz HM, Jokihaara J, Leppanen OV, Jarvinen T, Cooper DML. 3D visualization and quantification of rat cortical bone porosity using a desktop micro-CT system: a case study in the tibia. J Microsc. 2010; 240:32–37. [PubMed: 21050211]
22. Feldkamp LA, Davis LC, Kress JW. Practical cone-beam algorithm. J Opt Soc Am. 1984; 1:612–619.
23. Tommasini SM, Trinward A, Acerbo AS, De Carlo F, Miller LM, Judex S. Changes in intracortical microporosities induced by pharmaceutical treatment of osteoporosis as detected by high resolution micro-CT. Bone. 2012; 50:596–604. [PubMed: 22226688]
24. Hildebrand T, Ruegsegger P. A new method for the model-independent assessment of thickness in three-dimensions. J Microc. 1997; 185:67–75.
25. Gu XI, Palacio-Mancheno PE, Leong DJ, Borisov YA, Williams E, Maldonado N, Laudier D, Majeska RJ, Schaffler MB, Sun HB, Cardoso L. High resolution micro arthrography of hard and soft tissues in a murine model. Osteoarthritis Cartilage. 2012; 20:1011–1019. [PubMed: 22613702]
26. Duvall CL, Taylor WR, Weiss D, Guldberg RE. Quantitative microcomputed tomography analysis of collateral vessel development after ischemic injury. Am J Physiol Heart Circ Physiol. 2004; 287:H302–H310. [PubMed: 15016633]
27. Sietsema WK. Animal models of cortical porosity. Bone. 1995; 17:297S–305S. [PubMed: 8579932]
28. Schneider P, Krucker T, Meyer E, Ulmann-Schuler A, Weber B, Stampanoni M, Müller R. Simultaneous 3D visualization and quantification of murine bone and bone vasculature using micro-computed tomography and vascular replica. Microsc Res Tech. 2009; 72:690–701. [PubMed: 19360841]
29. Martín-Badosa E, Amblard D, Nuzzo S, Elmoutaouakkil A, Vico L, Peyrin F. Excised bone structures in mice: imaging at three-dimensional synchrotron radiation micro CT. Radiology. 2003; 229:921–928. [PubMed: 14657323]
30. Windhal SH, Vidal O, Andersson G, Gustafsson JA, Ohlsson C. Increased cortical bone mineral content but unchanged trabecular bone mineral density in female ERβ−/− mice. J Clin Invest. 1999; 104:895–901. [PubMed: 10510330]

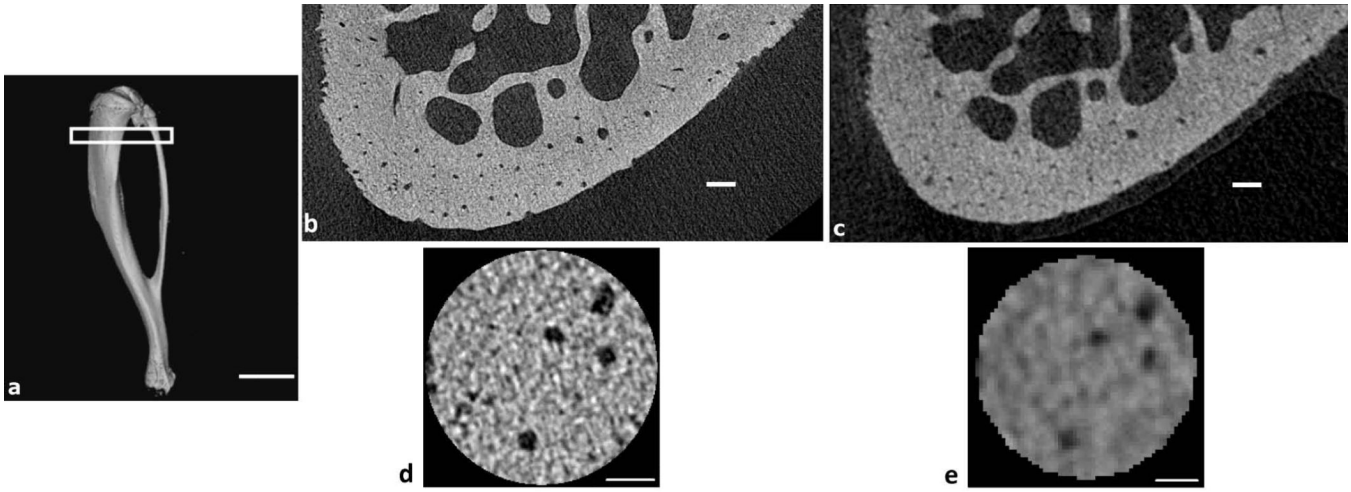

Fig. 1.

(a) µCT reconstruction of a whole rat tibia (4-µm resolution) demonstrating the region of analysis, starting 1 mm below the proximal growth plate (scale bar: 6 mm). **(b)** Reconstructed 1-µm resolution µCT image of the anterior proximal tibial metaphysis and **(c)** Reconstructed 4-µm resolution µCT image of the same region shown in (b) (scale bars: 100 µm). **(d)** A slice through a volume of interest (VOI) from a 1-µm resolution image and **(e)** from a 4-µm resolution image of the same region shown in (d) (scale bars: 50 µm).

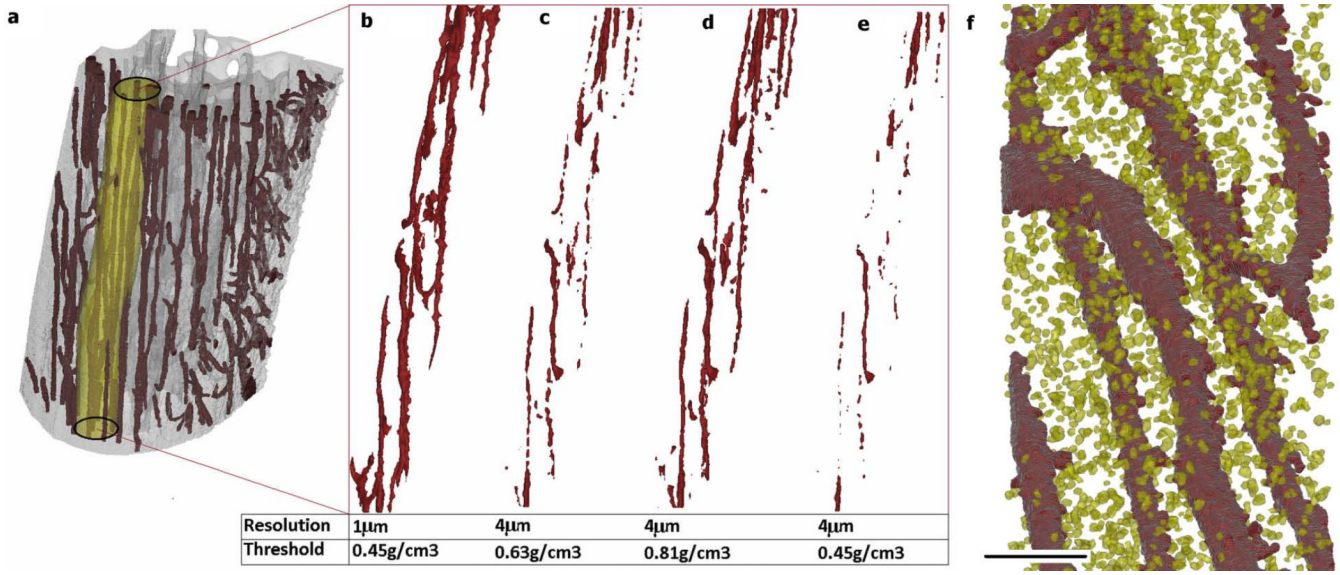

Fig. 2.

(a) 3D rendering of a µCT reconstruction of the anterior proximal tibia showing a 250-µm diameter cylindrical VOI used for analysis. 3D renderings of the analyzed VOI showing the vascular canal structure **(b)** at 1-µm resolution with threshold of 0.45 gHA/cm^3 (determined using Edge_Det and Hist threshold methods), **(c)** at 4-µm resolution with threshold of 0.63 gHA/cm^3 (determined using Edge_Det threshold method), **(d)** at 4-µm resolution with threshold of 0.81 gHA/cm^3 (determined using Hist threshold method), and **(e)** at 4-µm resolution with the density-based threshold determined using the 1-µm resolution scans (0.45 gHA/cm^3). **(f)** 3D rendering from a 1-µm resolution µCT reconstruction showing vascular canals (dark red) and osteocyte lacunae (yellow) (scale bar: 100 µm).

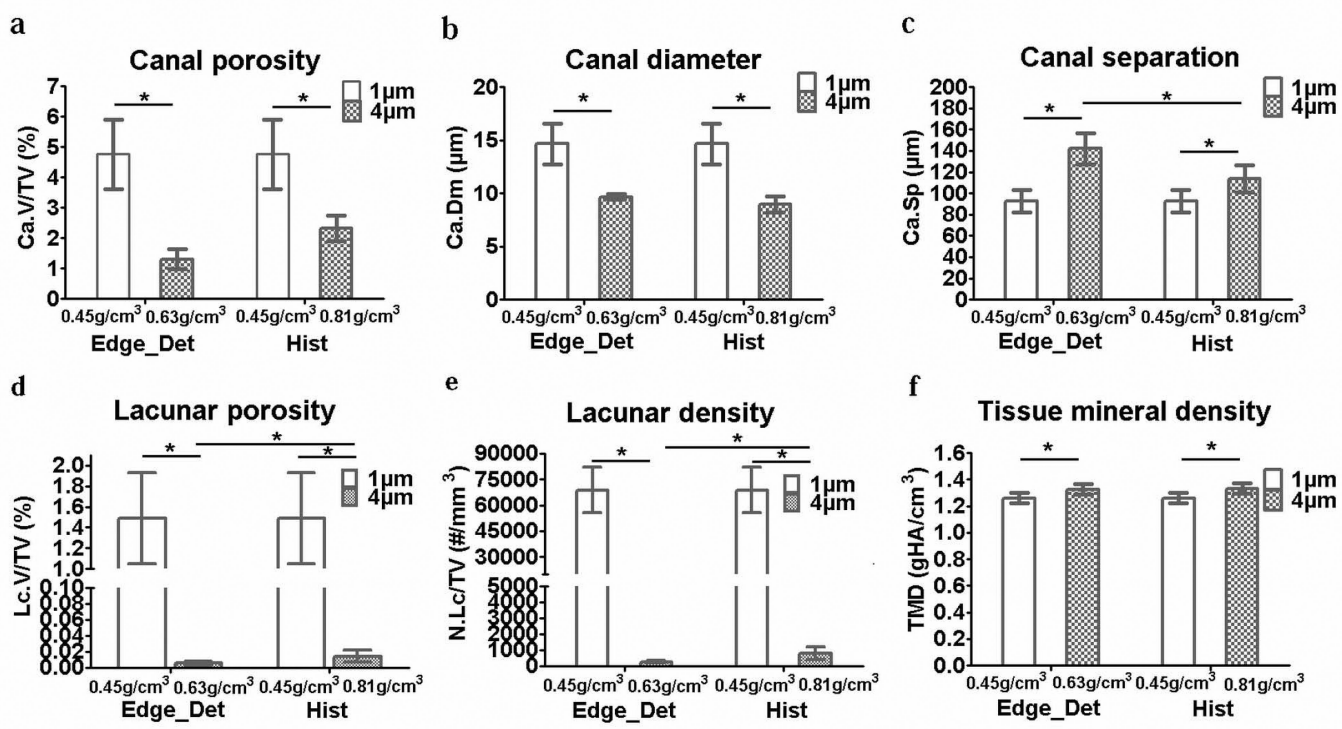

Fig. 3.

Bar plots (mean ± SD; n=6) indicating bone microarchitectural and TMD differences due to resolution (1-µm or 4-µm) and threshold method (Edge_Det or Hist method): **(a)** vascular canal porosity, **(b)** vascular canal diameter, **(c)** vascular canal separation, **(d)** osteocyte lacunar porosity, **(e)** osteocyte lacunar density and **(f)** tissue mineral density. *p<0.05

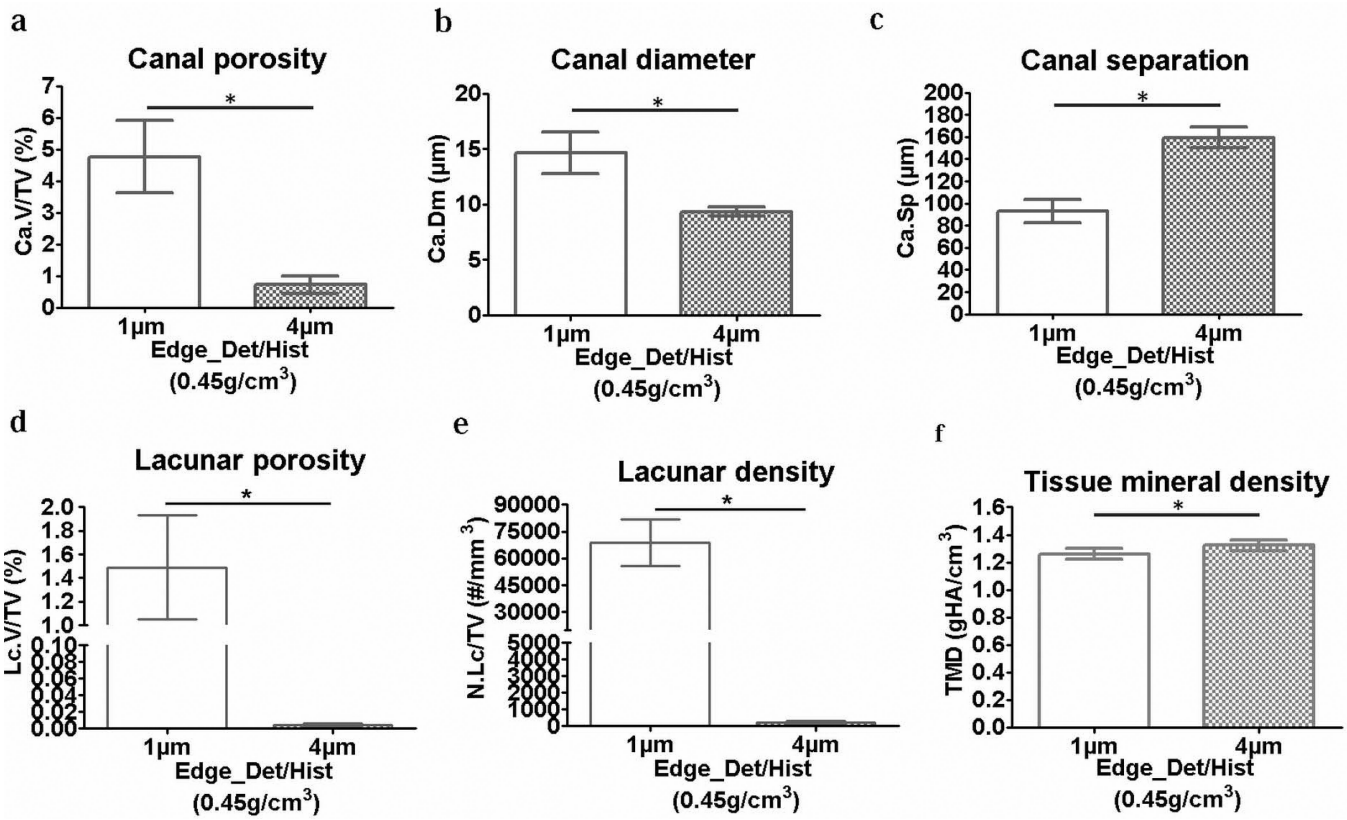

Fig. 4.

Bar plots (mean ± SD; n=6) indicating bone microarchitectural and TMD differences due to application of a high-resolution density-based threshold to both the 1-µm and 4-µm resolution scans: **(a)** vascular canal porosity, **(b)** vascular canal diameter, **(c)** vascular canal separation, **(d)** osteocyte lacunar porosity, **(e)** osteocyte lacunar density and **(f)** tissue mineral density. *p<0.05

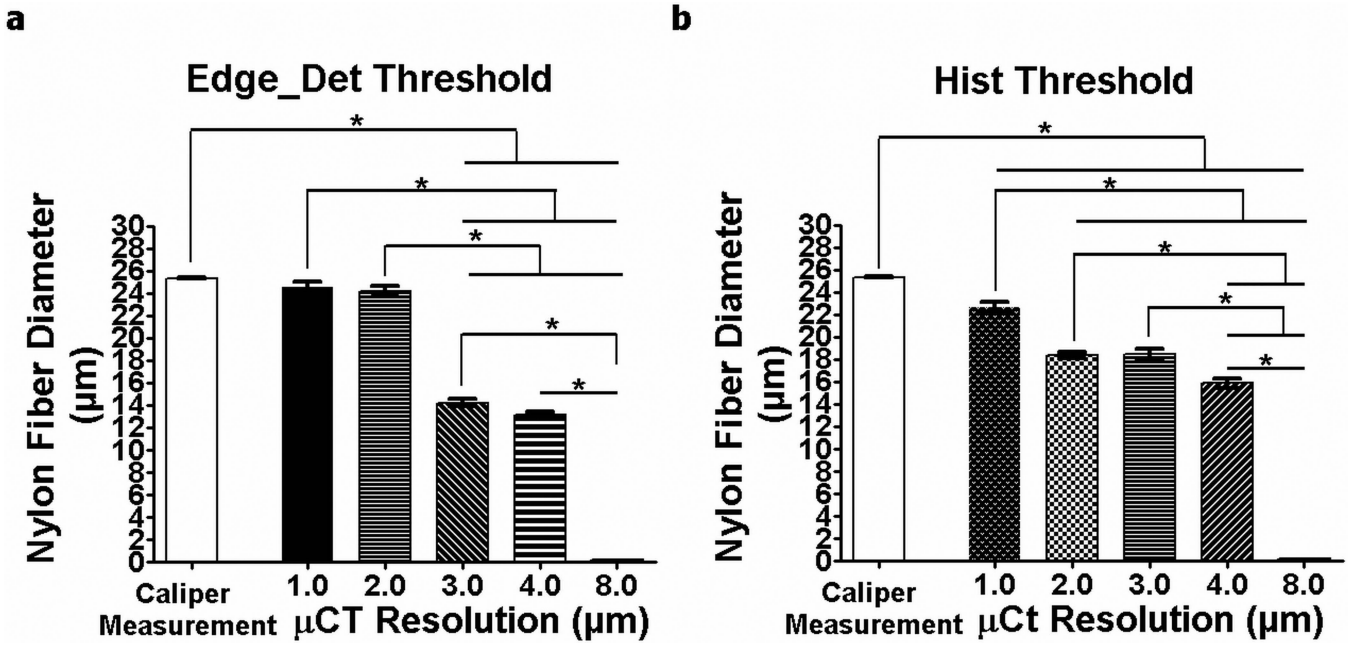

Fig. 5.

The diameter of nylon fibers (mean ± SD; n=7) measured using calipers as well as with µCT scans at resolutions ranging from 1 µm to 8 µm using **(a)** the Edge_Det threshold method and **(b)** the Hist threshold method. *$p < 0.05$

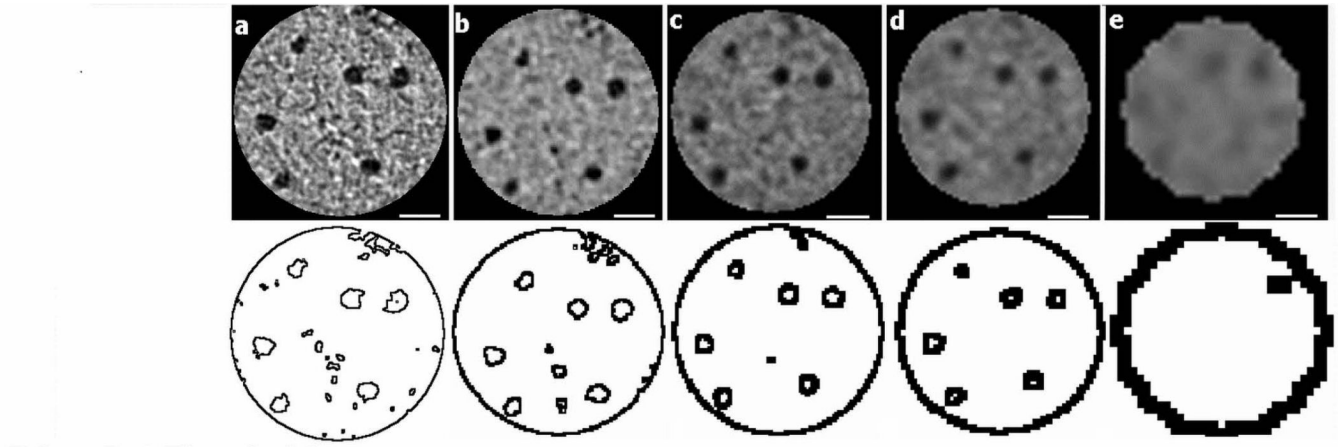

Edge_Det Threshold

Resolution	1 μm	2 μm	3 μm	4 μm	8 μm
Ca.Dm [μm]	22.2	21.1	19.1	15.2	0
N.Lc/TV [#/mm³]	42800	19000	1630	41	0
Lc.V/TV [%]	1.24	0.572	0.049	0.001	0

Hist Threshold

Resolution	1 μm	2 μm	3 μm	4 μm	8 μm
Ca.Dm [μm]	22.7	21.0	19.6	16.4	0
N.Lc/TV [#/mm³]	40700	16600	2700	103	0
Lc.V/TV [%]	1.20	0.482	0.079	0.004	0

Fig. 6.

μCT reconstructions of the same region of interest from the proximal anterior region of a rat tibia demonstrating the effects of scanning resolution, **(a)** 1-μm, **(b)** 2-μm, **(c)** 3-μm, **(d)** 4-μm and **(e)** 8 -μm resolution, on the vascular canal diameter (Ca.Dm), lacunar density (N.Lc/TV), and lacunar porosity (Lc.V/TV) using the Edge_Det and Hist threshold methods. The edge-detected images in the second row demonstrate the delineation of the vascular pores (the larger pores) and the osteocyte lacunar pores (the smaller pores) at each resolution. Scale bars: 50 μm.